EBioMedicine 31 (2018) 190–201

Contents lists available at ScienceDirect

EBioMedicine

journal homepage: www.ebiomedicine.com

Research Paper

The Novel Pathogenesis of Retinopathy Mediated by Multiple RTK Signals is Uncovered in Newly Developed Mouse Model

Hideyuki Kitahara [a,b], Sayaka Kajikawa [a], Yoko Ishii [a], Seiji Yamamoto [a,*], Takeru Hamashima [a], Erika Azuma [a,c], Hikari Sato [d], Takako Matsushima [a], Masabumi Shibuya [e], Yutaka Shimada [b], Masakiyo Sasahara [a,*]

[a] Department of Pathology, Graduate School of Medicine and Pharmaceutical Sciences, University of Toyama, 2630 Sugitani, Toyama-shi, Toyama 930-0194, Japan
[b] Department of Japanese Oriental Medicine, Graduate School of Medicine and Pharmaceutical Sciences, University of Toyama, 2630 Sugitani, Toyama-shi, Toyama 930-0194, Japan
[c] Department of Technology Development, Toyama Technology Center, Astellas Pharma Tech Co., Ltd., 2-178 Kojin-machi, Toyama-shi, Toyama 930-0809, Japan
[d] Department of Neurosurgery, Tokyo General Hospital, 3-15-2 Egota, Nakano-ku, Tokyo 165-0022, Japan
[e] Department of Research and Education, Jobu University, 634-1 Toyazuka-machi, Isesaki-shi, Gunma 372-8588, Japan

ARTICLE INFO

Article history:
Received 9 March 2018
Received in revised form 16 April 2018
Accepted 23 April 2018
Available online 25 April 2018

Keywords:
PDGF
PlGF
VEGF
Proliferative membrane
Pathological angiogenesis
Retinopathy

ABSTRACT

Pericyte desorption from retinal blood vessels and subsequent vascular abnormalities are the pathogenesis of diabetic retinopathy (DR). Although the involvement of abnormal signals including platelet-derived growth factor receptor-β (PDGFRβ) and vascular endothelial growth factor-A (VEGF-A) have been hypothesized in DR, the mechanisms that underlie this processes are largely unknown. Here, novel retinopathy mouse model (N-PRβ-KO) was developed with conditional *Pdgfrb* gene deletion by *Nestin* promoter-driven Cre recombinase (Nestin-Cre) that consistently reproduced through early non-proliferative to late proliferative DR pathologies. Depletion of Nestin-Cre-sensitive PDGFRβ$^+$NG2$^+$αSMA$^-$ pericytes suppressed pericyte-coverages and induced severe vascular lesion and hemorrhage. Nestin-Cre-insensitive PDGFRβ$^+$NG2$^+$αSMA$^+$ pericytes detached from the vascular wall, and subsequently changed into myofibroblasts in proliferative membrane to cause retinal traction. PDGFRα$^+$ astrogliosis was seen in degenerated retina. Expressions of placental growth factor (PlGF), VEGF-A and PDGF-BB were significantly increased in the retina of N-PRβ-KO. PDGF-BB may contribute to the pericyte-fibroblast transition and glial scar formation. Since VEGFR1 signal blockade significantly ameliorated the vascular phenotype in N-PRβ-KO mice, the augmented VEGFR1 signal by PlGF and VEGF-A was indicated to mediate vascular lesions. In addition to PDGF-BB, PlGF and VEGF-A with their intracellular signals may be the relevant therapeutic targets to protect eyes from DR.

1. Introduction

Retinopathy caused by diabetes mellitus is one of the major causes of vision impairment worldwide [10,48]. Microvascular degeneration including increased vascular permeability, microaneurysms and acellular capillaries as well as related ischemic damages are features of non-proliferative and early diabetic retinopathy (DR). Along the progress to proliferative DR, the risk of irreversible vision loss is increased due to macular oedema, hemorrhage, and proliferative membrane-mediated tractional retinal detachment [48]. Accordingly, for the protection and restoration of visual acuity, further studies are necessary that focus on the mechanism of disease progression from early non-proliferative to late proliferative DR.

Functional disturbance and apoptotic death of vascular cells are mediated by many mechanisms in early DR, among which, chronic disturbance of platelet derived growth factor receptor (PDGFR) β signal induced by sustained hyperglycemia importantly mediates pericyte injury that causes vascular abnormalities in DR [19]. Along this line, the vascular lesions of retina with decreased pericyte-coverage have been analyzed as a useful model of DR that were induced in hypomorphic mutant of *Pdgfb* or *Pdgfrb* genes or in the eyes treated with neutralizing antibody against PDGFRβ [7,25,33,37]. Besides these, PDGFs are augmented in DR, and PDGF-BB is specifically upregulated in proliferative DR [39]. PDGF is a mitogen of glial cells and mesenchymal cells including vascular pericytes [2,23]. Thus, PDGF may be involved in the formation of proliferative membrane and gliosis in proliferative DR, although the roles are remained unknown.

Vascular endothelial growth factor (VEGF)-A [15] that specifically binds VEGF receptors (VEGFRs) 1 and 2 is upregulated in DR in response to the ischemia induced by retinal vascular damage, and exacerbates extra-retinal vascular outgrowth to the retinal surface without amelioration of ischemia in the retina [18,31,35,44,48,50]. VEGF-A is the best characterized therapeutic target of DR, and anti-VEGF-A therapy significantly improved the prognosis of DR; however, significant part of

* Corresponding authors.
E-mail addresses: seiyama@med.u-toyama.ac.jp (S. Yamamoto), sasahara@med.u-toyama.ac.jp (M. Sasahara).

https://doi.org/10.1016/j.ebiom.2018.04.021

patients with DR insufficiently respond to this therapy [47]. Placental growth factor (PlGF) is another angiogenic growth factor of VEGF family that specifically binds VEGFR1 [11,36,49], and data have accumulated showing the increase of PlGF in the vitreous humour and retina of eyes with DR as reviewed [32]. Thus, PlGF is supposed as an additional intricate therapeutic target of DR; however the roles of PlGF as well as VEGFR1 in DR remain to be elucidated.

In the present study, we established a new retinopathy model mice (N-PRβ-KO mice) with the C57BL/6 genetic background, harboring the *Pdgfrb* gene flanked by two loxP sequences (*Pdgfrb*$^{flox/flox}$) and *Nestin* promoter-driven Cre recombinase. The phenotype of retinopathy is inherited with a high penetration rate, and the model consistently reproduces the early to late phases of DR pathologies, whereas these changes occurred in early periods of life. PDGFRα and PDGFRβ activated by increased PDGF-BB were indicated to be involved in astrogliosis and the formation of proliferative membrane in retinopathy, respectively. PlGF and VEGF-A were upregulated in retinopathy in N-PRβ-KO mice, and genetical blockade of VEGFR1 signal substantially ameliorated the retinal vascular lesions. Our findings uncovered the novel pathogenesis mediated by PDGF-BB-PDGFRs and PlGF/VEGF-A-VEGFR1 signal axes.

2. Materials and Methods

2.1. Conditional Knockout Mice

All experimental animal procedures were conducted according to the Institutional Animal Care and Use Committee at the University of Toyama (Sugitani, Toyama, Japan). All study protocols were approved by the Ethics Committee of the University of Toyama before the studies were performed.

We previously established a *Pdgfrb*$^{flox/flox}$ mouse line with the 129SV genetic background [17]. The congenic strain C57BL/6-Ly5.1 harboring *Nestin* promoter/enhancer-driven Cre recombinase was obtained (*Nestin-Cre*, Jackson Laboratories, Bar Harbor, ME, USA). In the present study, backcross mating was carried out for 15 generations between *Pdgfrb*$^{flox/flox}$ mice and wild-type (WT) C57BL/6 mice (Japan SLC, Shizuoka, Japan) and for 18 generations between *Nestin-Cre* mice and WT C57BL/6 mice. The resulting N-PRβ-KO offspring showed severe retinopathy phenotypes with a very high penetration rate. All mice were housed at 25 °C with a 12-h light/dark cycle with free access to pellet chow and water. Genotyping of the *Pdgfrb*$^{flox/flox}$ [17], *Nestin-Cre* [41], *R26R-mCherry* [23] and *Flt1TK*$^{-/-}$ [21] were performed by genomic PCR. The primer sequences are given in Supplementary information.

2.2. Immunofluorescence

For paraffin section and whole mount sample preparation, excised eyes were fixed with 4% paraformaldehyd at 4 °C overnight. Eyes were dehydrated with a graded series of ethanol solutions, and embedded in paraffin. The sections (5 μm in thickness) were subjected to immunofluorescence and hematoxylin and eosin (HE) staining. In whole mount analysis, retinas were peeled out, and then mmunofluorescence staining was performed as described previously [23,51,53]. Briefly, the specimens were incubated at 4 °C overnight with the appropriate primary and secondary antibodies. The details of antibodies are given in Supplementary Information. Specimens for immunofluorescence were observed using a LSM780 confocal system (Carl Zeiss, Oberkochen, Germany), a TCS SP5 confocal system (Leica, Heidelberg, Germany), and a BZ-X700 microscope (Keyence, Osaka, Japan). Images were appropriately processed using Photoshop software (version 7.0; Adobe, San Jose, CA, USA).

2.3. RNA Extraction, cDNA Synthesis, and Real-Time PCR

Total RNAs were isolated from retinas of N-PRβ-KO and WT mice using the miRNeasy Mini Kit (Qiagen, Valencia, CA, USA), and were reverse-transcribed according to the PrimeScript RT Reagent Kit protocol (TAKARA BIO INC., Shiga, Japan). cDNAs were diluted 1:25 in the reaction mixture consisting of SYBR Premix EX Taq II (TAKARA BIO INC.), and then real-time PCR performed using a TAKARA Thermal Cycler Dice Real Time System TP800 as previously described [52]. Induction values were calculated using analysis software (TAKARA BIO INC.). Primer sequences are available upon request from the TAKARA BIO INC. website (http://www.takara-bio.co.jp).

2.4. Western Blotting

Sample preparations and all other procedures for western blotting are described elsewhere [41,52]. Briefly, retinas were lysed using T-PER Tissue Protein Extraction Reagent (Thermo Fisher Scientific Inc.) on ice. Lysates were electrophoretically separated, and then transferred to polyvinylidene difluoride membranes. Skim milk blocked membranes were incubated with primary antibodies described in Supplementary Information, and then were incubated with the appropriate horseradish peroxidase-conjugated secondary antibodies. Immunoreactive bands were detected using enhanced chemiluminescence reagents (GE Healthcare Bio-Sciences AB, Uppsala, Sweden) according to the manufacturer's instructions.

2.5. Enzyme-Linked Immunosorbent Assay

The concentrations of PDGF-AB, PDGF-BB, VEGF-A, and PlGF in the retinas of N-PRβ-KO or WT mice were measured by ELISA according to the manufacturer's instructions (R&D, Minneapolis, MN, USA). Briefly, collected retinas were snap-frozen in liquid nitrogen, smashed into a powder using the Multi-Beads Shocker (Yasui-kiki, Osaka, Japan), and lysed using T-PER Tissue Protein Extraction Reagent (Thermo Fisher Scientific Inc., Waltham, MA, USA) with Halt Protease Inhibitor Cocktail (Thermo Fisher Scientific Inc.). After centrifugation, lysates were used as samples. The concentrations of PDGF-AB, PDGF-BB, VEGF-A, and PlGF were calculated from the standard curve.

2.6. Image Analysis and Quantification

Images of HE sections of retinas were captured using an IX71 microscope (Olympus) and the retinal thickness of the peripheral area was measured using cellSens Standard (ver.1.4.1; Olympus). Images of the whole mount retinas were captured using a LSM780 confocal system (Carl Zeiss) and a BZ-X700 microscope (Keyence). Percentage of the immunoreactivity of CD31 and collagen type IV (pixel) in whole retinal area (pixel) were analyzed using BZ-H3C software (Keyence). For pericyte coverage on the retinal vasculature, the percentage of area that was immunoreactive (pixel) for NG2, CD13 and CD31 was analyzed using ImageJ (National Institutes of Health, Bethesda, MD, USA). For the analysis of western blotting data, the immunoreactive bands were quantified using ImageJ (NIH) and normalized to the β-actin band.

2.7. Statistical Analysis

All values are presented as means ± SEM. Statistical analyses of differences between groups were performed using Student's *t*-tests or one- or two-way analyses of variance (ANOVA) with Tukey's multiple comparison tests for post-hoc analysis were used. A p-value of <0.05 was considered statistically significant. Graphs were drawn using GraphPad Prism 6 software (GraphPad Software, Inc., La Jolla, CA, USA).

3. Results

3.1. N-PRβ-KO Mice Show Pathological Vascular Remodeling and Tractional Retinal Detachment

N-PRβ-KO mice with conditionally depleted *Pdgfrb* (Fig. 1a) grew to the adult stage and fertile without visible structural abnormalities in the

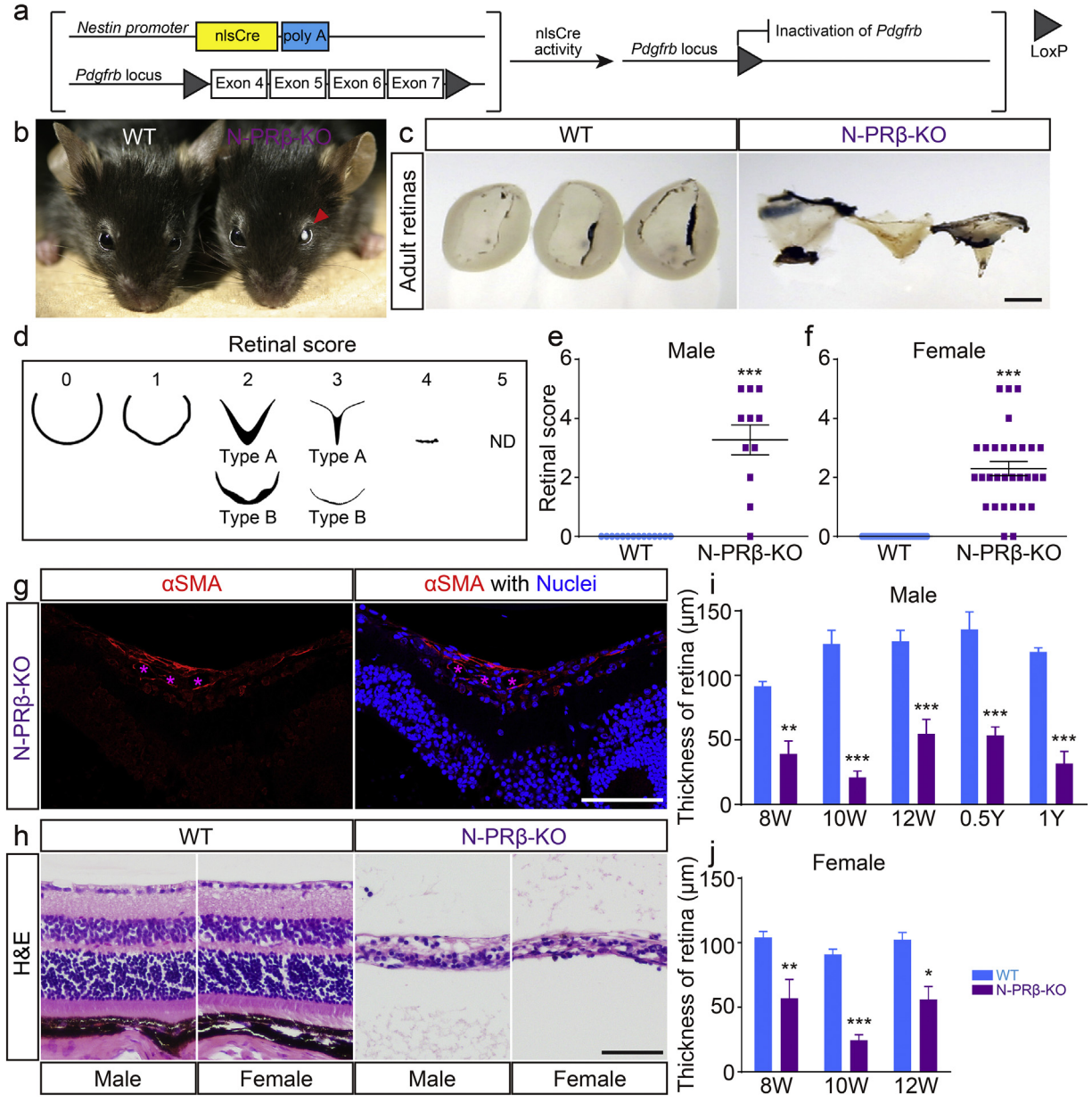

Fig. 1. N-PRβ-KO mice show severe retinal structural defects in adult mice. (a) Schematic representation of the transgenic and mutated alleles of N-PRβ-KO. Exons 4 to 7 of the *Pdgfrb* gene flanked by two loxP sites are deleted by nlsCre activity driven by the *Nestin* promoter. (b and c) N-PRβ-KO mice showed vitreous opacity (b, red arrowhead) and detached retina (c) compared with wild-type (WT) mice at 8–12 weeks old. (d) Scoring of retinal deformities. 0, normal cup-shaped retina; 1, distorted cup-shaped retina; 2, detached V-shaped retina or shrunken retina; 3, highly detached V-shaped and very thin peripheral retina or highly shrunken and very thin retina; 4, rudimentary retina; 5, not detected. (e and f) Both male (e) and female (f) N-PRβ-KO mice showed higher deformity scores at 8–12 weeks old than those of WT mice. $n = 11$–14 male retinas, $n = 30$–33 female retinas. (g) Typical proliferative membrane on the retinal surface of N-PRβ-KO mice at 10 weeks old. The proliferative membrane includes αSMA-positive cells (red) and blood vessels (indicated by asterisks in magenta). Hoechst staining depicts nuclei (blue). (h) Histology (H&E staining) of the peripheral region of the N-PRβ-KO retina at 10 weeks old. Highly perturbed thin retinas are observed compared to WT retinas. (i and j) N-PRβ-KO showed significantly thinner retinas than those of WT mice for both males (i) and females (j) in the adult stage. $n = 5$–8 males and females. All values represent means ± SEM. *, $p < 0.05$; **, $p < 0.01$; ***, $p < 0.001$, compared to WT mice at the same time points. Scale bar = 1 mm (c), 100 μm (g and h).

organ such as brain and kidney (Fig. S1), but except in their eyes, and blood glucose levels were not altered (118.6 ± 7.9, 118.4 ± 15.3, 117.9 ± 5.0, and 111.5 ± 4.0 mg/dL in male and female N-PRβ-KO mice and male and female wild-type (WT) mice, respectively, at 4 weeks of age). Most of these mutants exhibited vitreous opacity in bilateral eye in the adult stage (8 to 12 weeks of age; Fig. 1b). Tractional retinal detachment with an abnormal shape was characteristic of N-PRβ-KO mice, but was not seen in WT mice (Fig. 1c). Arbitrary scoring of the retinal shape abnormality indicated that >90% of N-PRβ-KO mice showed some degree of retinal injury, and male and female mice were similarly affected (Fig. 1d–f). The tractional retinal detachment was histologically identified as a V-shaped deformity of the retina. It is of note that an αSMA^+ proliferative membrane was identified on the retinal surface of this deformity (Fig. 1g). The normal layered structures of the retina were highly destroyed, resulting in the thinning of the peripheral area of the retina in N-PRβ-KO mice (Fig. 1h). This thinning in male and female N-PRβ-KO mice was significant at 8 weeks old, and remained at similar levels until 1 year of age (Fig. 1i and j). The disruption of the retina was essentially established at 8 weeks of age.

Pericyte loss occurs at the earliest stages of DR and can trigger subsequent pathological vascular remodeling, consisting of angiogenesis and vascular regression. ECM deposition is also eventually involved. Based on the whole-mount view of the isolated retina, the density of $CD31^+$ blood vessels appeared higher in N-PRβ-KO mice than in WT mice

(Fig. 2a, upper row). Increased CD31$^+$ staining in N-PRβ-KO mice was confirmed morphometrically in both sexes, to a similar extent (Fig. 2b and c). Collagen type IV staining was greater in N-PRβ-KO than in WT mice (Fig. 2a, bottom row) and the difference between the two genotypes was significant based on a morphometric analysis (Fig. 2d and e). Similar results were obtained for both genders. Based on observations at a high magnification, CD13$^+$ pericytes drastically disappeared around the CD31$^+$ retinal blood vessels of N-PRβ-KO mice compared to WT mice (Fig. 2f). Accordingly, the percentage of pericyte coverage was substantially decreased in retinal vessels of N-PRβ-KO mice, irrespective of gender (Fig. 2g and h). Furthermore, many collagen type IV$^+$/CD31$^-$ structures, corresponding to empty sleeves [45],

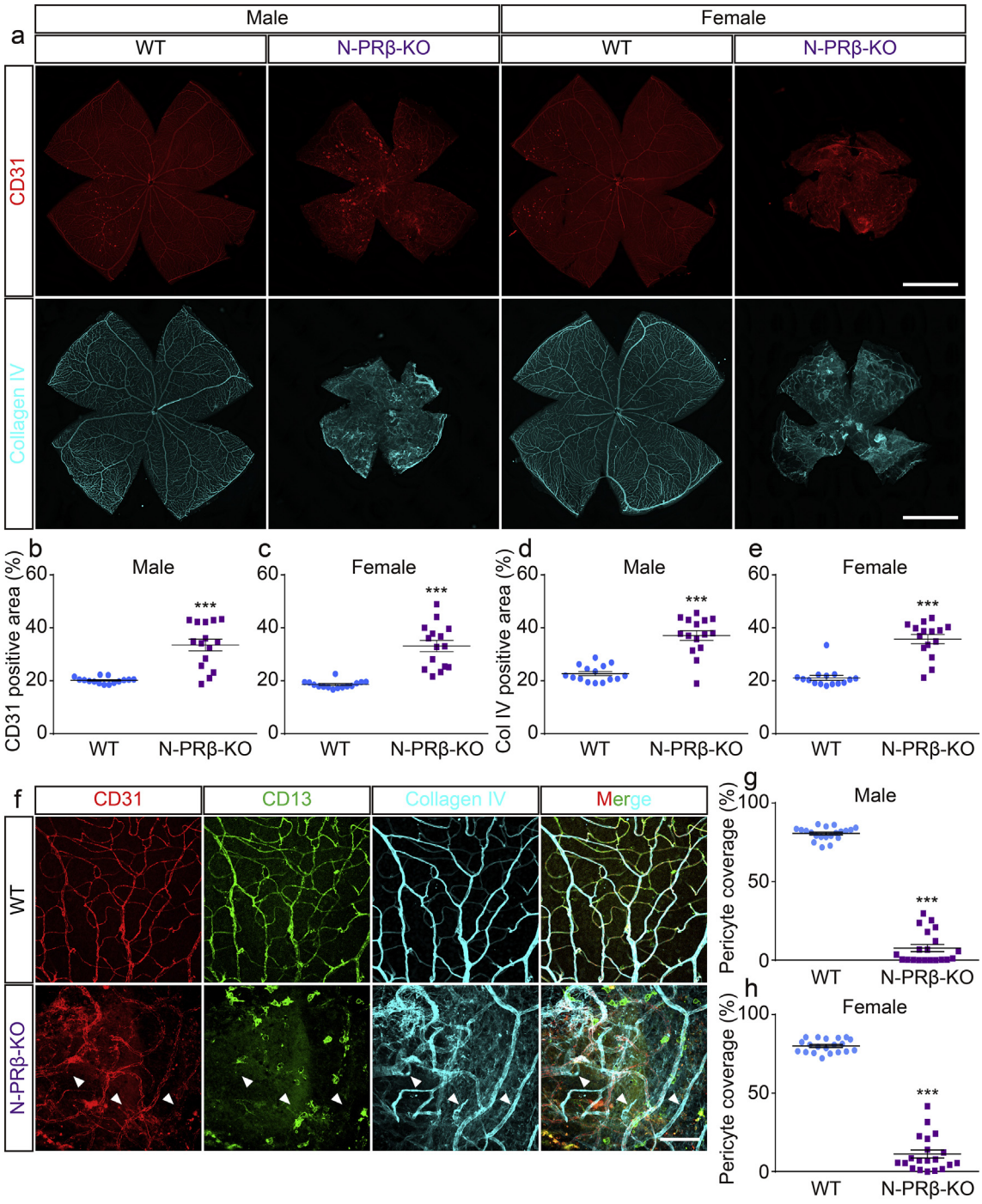

Fig. 2. N-PRβ-KO adult mice show severe retinal blood vessel defects. (a) N-PRβ-KO mice show retinal blood vessel defects in both males and females at the adult stage (8–12 weeks old). Immunofluorescence of CD31 (red) and collagen type IV (cyan) depict retinal vasculature and blood vessel specific ECM deposition of N-PRβ-KO mice compared with WT. (b and c) Ratio of the CD31-positive area compared to the whole area of the retina. N-PRβ-KO mice showed significantly higher ratios for both males (b) and females (c) compared with WT in the adult stage. $n = 15$ for males and females. (d and e) Ratio of the collagen type IV-positive area compared to the whole area of the retina. N-PRβ-KO mice showed significantly higher ratios for both males (d) and females (e) compared with WT in the adult stage. n = 15 for males and females. (f) Multi-colour representative immunofluorescence images of WT (upper row) and N-PRβ-KO mice (bottom row) at 10 weeks old. CD31-positive blood vessels (red), CD13-positive pericytes (green), collagen type IV deposition (cyan). Arrowheads indicate empty sleeves. (g and h) Percentage of pericyte coverage on the retinal vasculature of N-PRβ-KO mice. N-PRβ-KO mice showed significantly lower coverage rates for both males (g) and females (h) compared with WT in the adult stage. $n = 20$ randomly selected areas (20× objective lens) from 5 retinas of males and females. All values represent the mean ± SEM. ***, $p < 0.001$, compared to WT. Scale bar = 1 mm (a), 100 μm (f).

indicated vascular regression in N-PRβ-KO mice, but not in WT mice (Fig. 2f, arrowheads). These collagen structures and abnormal vascular branches (Fig. 2f) may contribute to the increased measurement of CD31 and collagen type IV positive areas in N-PRβ-KO mice (Fig. 2b–e). PDGFRβ null embryos show pericyte coverage deficiency [20]. To confirm whether the severe depletion of pericytes in N-PRβ-KO mice was a consequence of Cre recombinase-mediated *Pdgfrb* gene knockout, we conducted a fate mapping study utilizing *Nestin-Cre;R26R-mCherry* mice (N-MC, Fig. S2a). Many, but not all pericytes expressed mCherry of the retinal blood vessels in N-MC mice (Fig. S2b–d, magenta-arrowheads). The mCherry$^+$ pericytes significantly outnumbered mCherry$^-$ pericytes in arterioles and capillaries in N-MC mouse retina (Fig. S2e and g). In contrast, mCherry$^-$ pericytes significantly outnumbered mCherry$^+$ pericytes in venules of the N-MC mice (Fig. S2f). These findings indicate that *Pdgfrb* knockout in retinal pericytes in N-PRβ-KO mice resulted in severe depletion of retinal pericytes.

PDGFRβ insufficiency in pericytes induced proliferative DR-like lesions, including tractional retinal detachment associated with the proliferative membrane, and vascular phenotypes consisting of angiogenesis and regression in adult N-PRβ-KO mice. These data prompted us to investigate N-PRβ-KO mice at an earlier age to elucidate the developmental mechanism of the retinal lesion.

3.2. Retinal Degeneration was Induced by Hypoperfusion in N-PRβ-KO Mice

The thickness of the retina in N-PRβ-KO mice was comparable with that of WT mice until 10 days after birth, and then gradually decreased, becoming significantly less than that of WT at 8 weeks old (Fig. S3a). CD31$^+$ microvessels were dilated, and the extent of branching of the microvessels decreased (Fig. S3b). Vascular regression indicated by the empty sleeve was a prominent feature in N-PRβ-KO mice (Fig. S3b). Similarly non-functioning retinal vessels were often observed in N-PRβ-KO but not in WT mice (Fig. S3c). These indicate that the vascular regression-mediated local hypoperfusion is the underlying mechanism of the current retinopathy as has been demonstrated in DR [45]. In accordance with these, hypoperfusion-induced oxidative stress [6] was detected in retinopathy of N-PRβ-KO mice. 8-OHdG, an oxidative stress marker, was detected in glutamine synthetase$^+$ Müller cells, recoverin$^+$ photoreceptors, PKCα$^+$ bipolar cells, calretinin$^+$ amacrine cells, and calbindin$^+$ horizontal cells in the inner nuclear layer of the retina of 2 weeks old N-PRβ-KO (Fig. S4a–e). Whereas TUNEL-positive apoptotic cells did not co-localize 8-OHdG in N-PRβ-KO at this time point (data not shown), 8-OHdG was clearly co-expressed with SQSTM1 (Fig. S4f), an autophagy marker, suggesting that oxidative stress-induced autophagic cell death underlies the structural destruction and thinning of the retina after vascular phenotypes, e.g., dilatation and regression, are detected in N-PRβ-KO mice.

3.3. Molecular Mechanisms Underlying Retinal Detachment in N-PRβ-KO Mice

The deformation of the retina represented by a "retinal score" (Fig. 1d) was not significant at 1 week old, became significant at 2 weeks old and was further aggravated at 4 weeks old in both sexes of N-PRβ-KO mice as compared with WT mice (Fig. S5a and b). Immunofluorescence of whole mount retinal specimens showed that the network of CD31$^+$ blood vessels associated with αSMA$^+$ pericytes spread at 1 week, and a hierarchical vascular tree was established after 3 weeks in WT retina (Fig. 3a–c, left). Comparing to these, blood vessels were irregularly dilated, and αSMA$^+$ pericytes aberrantly distributed in association with capillaries at 1 week of age in N-PRβ-KO retina (Fig. 3a, right). Notably, triple-colour immunofluorescence at this time point demonstrated that almost all NG2$^+$αSMA$^-$ microvascular pericytes disappeared but NG2$^+$αSMA$^+$ pericytes still observed in microvasculatures of N-PRβ-KO compared to same region of WT (Fig. S5c). At 2 weeks of age, increased CD31 staining indicated increased angiogenesis with an irregular network pattern, vascular dilatation, and microaneurysm in N-PRβ-KO retina (Fig. 3b, right). These vascular phenotypes were frequently accompanied by large hemorrhages (Fig. S5d). Noteworthy, foci of the proliferative membrane consisted by αSMA$^+$ cells appeared at 2 weeks (Fig. 3b, right, arrowhead) and increased at 4 weeks (Fig. 3c, right, arrowheads), that could underlie the retinal deformation detected in these periods (Fig. S5a and b).

At the higher-magnification views, full coverage of NG2$^+$ pericytes on the blood vessels was observed in the WT retina at 4 weeks of age (Fig. 3d, upper row). Noteworthy, NG2$^+$αSMA$^-$ pericytes were exclusively located in the microvasculature (Fig. 3d, upper row, green-arrowheads), and NG2$^+$αSMA$^+$ pericytes preferentially enwrapped the arterioles, venules, and their primary branches (Fig. 3d, upper row, magenta-arrowheads). In age-matched N-PRβ-KO retinas, NG2$^+$αSMA$^-$ microvascular pericytes were also severely depleted (Fig. 3d, bottom row, green-arrowheads), whereas considerable number of NG2$^+$αSMA$^+$ pericytes were distributed along the microvasculature (Fig. 3d, bottom row, magenta-arrowheads). This depletion of NG2$^+$αSMA$^-$ microvascular pericytes corresponded to the decreased pericyte coverage of blood vessels (Fig. S6a and b), that is one of the most important vascular lesions of DR. Besides that, the proliferative membrane included many αSMA$^+$ cells and irregularly aggregated microvasculatures (Fig. S6c). These observations strongly suggest that NG2$^+$αSMA$^+$ pericytes in N-PRβ-KO are Nestin-Cre-insensitive pericyte subset (it means *Pdgfrb* preserving pericyte subset), and such pericyte subset may correspond to Nestin-Cre-insensitive mCherry$^-$αSMA$^+$ pericytes (Fig. S2). These cells often detached from blood vessels to become NG2$^-$αSMA$^+$ pericytes after complete detachment (Fig. S6d). Thereafter, they may change into myofibroblasts and may contribute to the formation of the proliferative membrane, in which the foci of proliferative membranes expressed collagen type I and connective tissue growth factor (CTGF) that are well-known factors for involving in the tissue fibrosis (Fig. S6e–h). Such issue will be further verified in following Fig. 5b–d.

To determine the molecular mechanisms underlying proliferative membrane formation in N-PRβ-KO retinas, the expression levels of PDGFs and receptors were examined, which are reportedly involved in fibroblast migration [17] and pericyte detachment [24]. Based on real-time PCR analyses, *Pdgfb* mRNA expression in the retina was significantly higher in N-PRβ-KO mice than in WT mice at 2 weeks old (Fig. 4b), and the mRNA expression levels of other PDGF ligands were comparable between the two genotypes (Fig. 4a–d). Similarly, based on ELISA, the expression of PDGF-BB, but not PDGF-AB, increased substantially at 2 weeks old and remained at a high level at 4 weeks old in the N-PRβ-KO retina (Fig. 4e and f). *Pdgfra* mRNA expression was significantly higher in N-PRβ-KO retinas than WT retinas at 2 weeks old and remained at a high level at 4 weeks old (Fig. 4g). *Pdgfrb* mRNA was significantly lower in N-PRβ-KO retinas than WT retinas at 1–4 weeks old (Fig. 4h). Similarly, increased PDGFRα and decreased PDGFRβ were detected in N-PRβ-KO retinas compared to WT retinas by western blotting (Fig. 4i and j). In immunofluorescence, PDGFRα was localized in a few GFAP$^+$ astrocytes in the ganglion cell layer of WT mice. In N-PRβ-KO retinas, increased PDGFRα was distributed on many glial scar-forming hypertrophic GFAP$^+$ astrocytes; the glial scar might contribute to tractional retinal detachment (Fig. 5a), as previously suggested [42]. PDGFRβ was still expressed in αSMA$^+$ pericytes, but was mostly suppressed in detached αSMA$^+$ pericytes of N-PRβ-KO mice (Fig. 5b, arrowheads). Fate mapping in *Nestin-Cre*;*Pdgfrb*$^{flox/flox}$;*R26R-mCherry* (N-PRβ-KO-MC, Fig. 5c) showed mCherry$^-$αSMA$^+$ detaching pericytes (Fig. 5d, green-arrowheads), which correspond to Nestin-Cre-insensitive mCherry$^-$αSMA$^+$ pericytes as shown in Fig. S2. These findings, together with Fig. S6d, strongly suggested that Nestin-Cre-insensitive PDGFRβ$^+$NG2$^+$αSMA$^+$ pericytes were incorporated into proliferative membrane through pericyte-fibroblast transition (PFT), and that this process appeared to be driven by PDGF-BB-PDGFRβ signal axis.

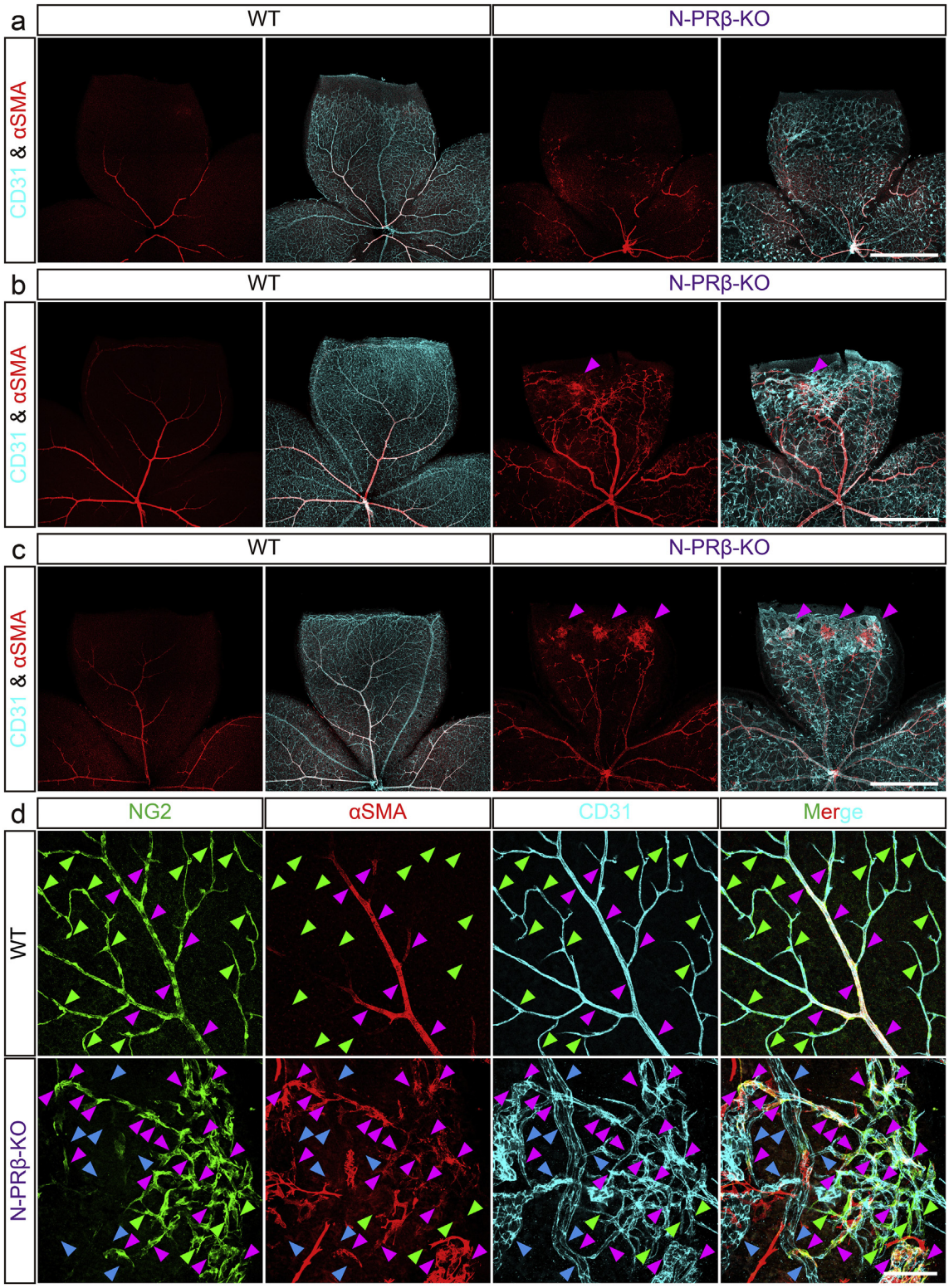

Fig. 3. Foci of proliferative membrane and structural abnormality of blood vessels are observed in early stage of N-PRβ-KO mouse retina. (a–c) Retinal angiogenesis of WT and N-PRβ-KO at 1 week (a), 2 weeks (b) and 4 weeks (c). CD31$^+$ retinal vascular networks (cyan) develop toward the peripheral region. αSMA$^+$ pericytes (red) that preferentially reside on the arteriole and venule are observed (a–c, left) in WT retinas. Owing to a loss of NG2$^+$αSMA$^-$ microvascular pericytes, N-PRβ-KO retina at 1 week show relatively large-sized capillaries. Additionally, defects in the specification of arterioles and venules are often observed, and atypical migration of NG2$^+$αSMA$^+$ pericytes can be found (a, right). Blood vessel dilation and microvascular aneurisms are often observed at 2 to 4 weeks. At the same time points, foci of proliferative membrane constituted by αSMA$^+$ pericytes (magenta-arrowheads, myofibroblast-like phenotype) are observed (b and c, right). (d) Multi-colour representative immunofluorescence images of WT (upper row) and N-PRβ-KO mice (bottom row) at 4 weeks. NG2$^+$ pericytes (green), αSMA$^+$ pericytes (red), CD31-positive blood vessels (cyan). In WT, whereas NG2$^+$αSMA$^+$ pericytes are preferentially observed on arterioles, venules and their primary branches (magenta-arrowheads), NG2$^+$αSMA$^-$ pericytes are exclusively observed on the capillaries (green-arrowheads). In N-PRβ-KO, considerable NG2$^+$αSMA$^+$ pericytes are observed on microvasculature (magenta-arrowheads) instead of NG2$^+$αSMA$^-$ pericytes (green-arrowheads). In addition, naked blood vessels are often observed (blue-arrowheads). Scale bar = 1 mm (a–c), 100 μm (d).

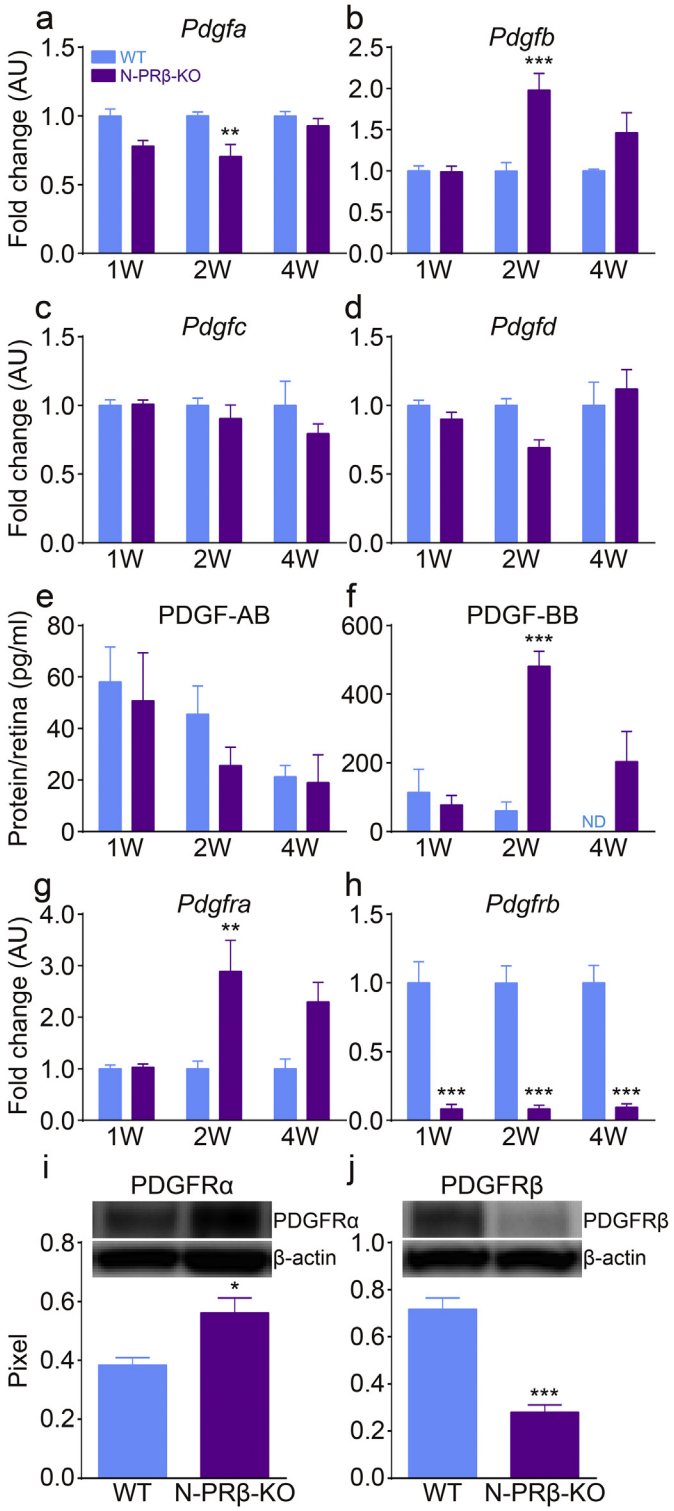

3.4. Molecular Mechanisms Underlying Pathological Angiogenesis in N-PRβ-KO Mice

To clarify underlying cellular and molecular mechanisms of pathological angiogenesis observed in the N-PRβ-KO retinas, we next examined the angiogenic factors corresponding to the above vascular phenotype. Among the major angiogenic factors examined, *Vegfa* mRNA tended to be higher in N-PRβ-KO than in WT retinas at 1–2 weeks old (Fig. 6a). *Plgf* mRNA in N-PRβ-KO retinas increased after 2 weeks, and the difference between the two genotypes was significant at 4 weeks (Fig. 6e). The mRNA expression levels were comparable between the two genotypes or tended to be lower in N-PRβ-KO than in WT retinas for all other VEGF ligands (Fig. 6b–d). Receptors for VEGF family were comparable between the two genotypes or tended to be lower in N-PRβ-KO than in WT retinas (Fig. 6f–h). Consistent with these results, VEGF-A protein expression was significantly higher at 2 weeks (Fig. 6i) and PlGF protein expression was significantly higher at 2 and 4 weeks (Fig. 6j) in N-PRβ-KO retinas than WT retinas.

PlGF exclusively binds and transduce intracellular signaling via VEGFR1 [11,49]. VEGF-A also binds VEGFR1, which plays an important role in development [16,21]. Accordingly, to understand the effects of increased PlGF and VEGF-A in N-PRβ-KO retinas, intracellular signaling via VEGFR1 was blocked in N-PRβ-KO mice by cross-breeding with *Flt1TK*$^{-/-}$ mice [21]. In *Flt1TK*$^{-/-}$ mice, no distinct vascular abnormalities could be observed in retinas compared to WT in physiological condition (Fig. S7). In pathological condition of retina shown in N-PRβ-KO, whereas no explicit changes were observed in aberrant migration of αSMA^{+} pericytes, formation of the proliferative membrane, and retinal structural destruction and thinning between N-PRβ-KO and N-PRβ-KO-Flt1TK$^{-/-}$ retinas, severely dilated blood vessels were restored to normal sized blood vessels in N-PRβ-KO-Flt1TK$^{-/-}$ retinas (Fig. 7a and b). Furthermore, the excessive deposition of collagen type IV in N-PRβ-KO retinas was decreased in N-PRβ-KO-Flt1TK$^{-/-}$ retinas (Fig. 7b). Increases in angiogenesis and vessel diameter in N-PRβ-KO retinas were significantly restored in N-PRβ-KO-Flt1TK$^{-/-}$ retinas (Fig. 7c and d). Moreover, increase in collagen type IV deposition in N-PRβ-KO retinas was significantly restored in N-PRβ-KO-Flt1TK$^{-/-}$ retinas (Fig. 7e and f). Accordingly, VEGFR1 signal activated by PlGF or VEGF-A is involved in pathological angiogenesis with a large hemorrhagic phenotype in retinopathy of N-PRβ-KO mice.

4. Discussion

Pericyte desorption from blood vessels mediated by insufficient PDGFRβ signal is followed by subsequent vascular abnormalities in DR. In a meanwhile, VEGFs in retina induced by hypoxia mediate proliferative DR [3]. These processes of disease progress were consistently represented in our mouse model with conditional *Pdgfrb* gene targeting by *Nestin* promoter-driven Cre. In N-PRβ-KO mice, blood vessels with severely decreased pericyte-coverage showed abnormal vascular dilatation, regression and hemorrhages. These were followed by changes like proliferative DR including angiogenesis, gliosis and proliferative membrane formation with tractional retinal detachment. Furthermore, VEGF-A was augmented in degenerated DR with oxidative stress and autophagic responses as reported in DR [43]. Accordingly, we examined

Fig. 4. The molecular mechanisms underlying tractional retinal detachment.(a–d) Real-time PCR analyses of PDGF ligands. *Pdgfb* mRNA (b) expression at 2 weeks was exclusively and significantly higher in N-PRβ-KO mice compared to that in WT mice. *Pdgfa* (a), *Pdgfc* (c), and *Pdgfd* (d) mRNA expression levels in N-PRβ-KO mice were similar or lower than the levels observed in WT mice. $n = 8$ at the indicated time points. (E and F) ELISA data for retinas at 1 to 4 weeks. PDGF-AB (e) expression was comparable between the two genotypes. PDGF-BB (f) expression in N-PRβ-KO was significantly higher at 2 weeks and tended to be higher at 4 weeks than that of WT mice. n = 5–7 at the indicated time points. (g and h) Real-time PCR analyses of PDGFRs expression. *Pdgfra* mRNA (g) expression in N-PRβ-KO was significantly higher at 2 weeks and tended to higher at 4 weeks than that of WT mice. *Pdgfrb* mRNA (h) expression in N-PRβ-KO was significantly lower at all time points than those in WT mice. n = 8 at the indicated time points. (i and j) Western blotting data of retinas at 2 weeks. PDGFRα protein (i) expression was significantly higher in N-PRβ-KO than that in WT mice. PDGFRβ protein (j) expression was significantly low level in N-PRβ-KO compared to WT mice. n = 5 in both genotypes. All values represent means ± SEM. *, $p < 0.05$; **, $p < 0.01$; ***, $p < 0.001$ vs. WT mice at the same time points. ND indicates not detected.

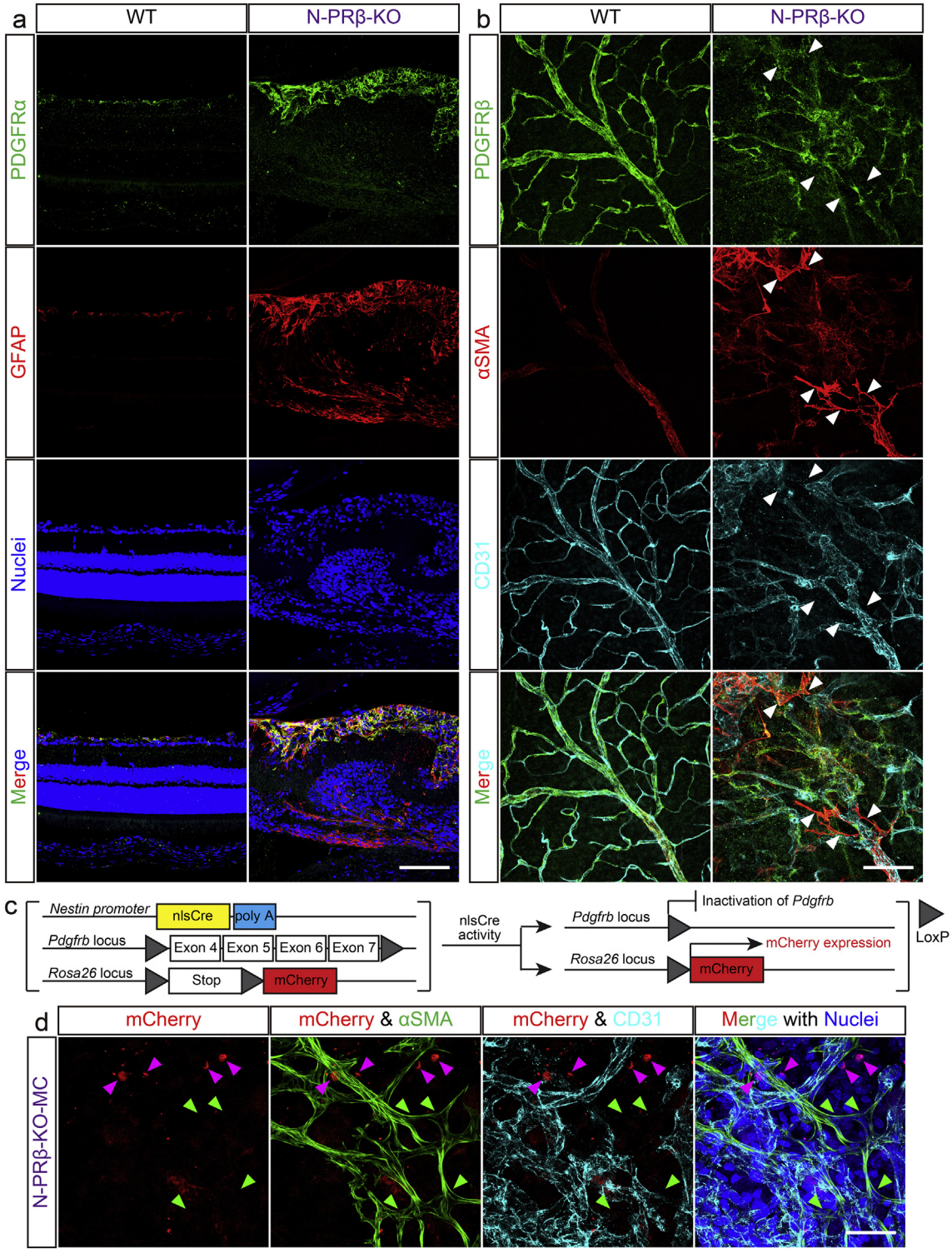

Fig. 5. Immunofluorescence analyses of N-PRβ-KO and N-PRβ-KO-MC mice. (a) In an immunofluorescence analysis, PDGFRα (green) is expressed on GFAP-positive astrocytes (red) in WT and N-PRβ-KO mice at 4 weeks. However, astrocytes of N-PRβ-KO mice are hypertrophic compared with WT mice. Hoechst-stained nuclei (blue). (b) Based on an immunofluorescence analysis, PDGFRβ (green) was expressed on both αSMA^{-} and αSMA^{+} pericytes (red) in WT mice at 4 weeks. Because $NG2^{+}\alpha SMA^{+}$ microvascular pericyte recruitment is observed in N-PRβ-KO mice, PDGFRβ (green) is preferentially expressed on αSMA^{+} pericytes (red) at 4 weeks. Arrowheads indicate αSMA^{+} pericytes detached from blood vessels suppressing PDGFRβ expression. (c) Schematic representation of the transgenic and mutated alleles of N-PRβ-KO-MC. Exons 4 to 7 of *Pdgfrb* flanked by two loxP sites are deleted by nlsCre activity driven by the *Nestin* promoter. At the same time, mCherry expression is driven by the *Rosa26* promoter, when two loxP sites flanking the stop codon are deleted by nlsCre activity. (d) In N-PRβ-KO-MC retinas at 2 weeks, αSMA^{+} pericytes detached from blood vessels (green, indicated by green-arrowheads) never express mCherry. Some $mCherry^{+}$ cells (red, indicated by magenta-arrowheads) are observed around the blood vessels (cyan), but not express αSMA. Hoechst-stained nuclei (blue). Scale bar = 100 μm (a and b), 50 μm (d).

the key molecules and mechanisms underlying mouse retinopathy; these results have implications for the prevention and care of DR, a major cause of vision-impairment worldwide [10,48].

Diabetes-induced pericyte reduction was not sufficient to provoke proliferative DR in rodents [26,29]. In contrast, severe pericyte depletion after the disturbance of PDGFRβ signal induced retinal

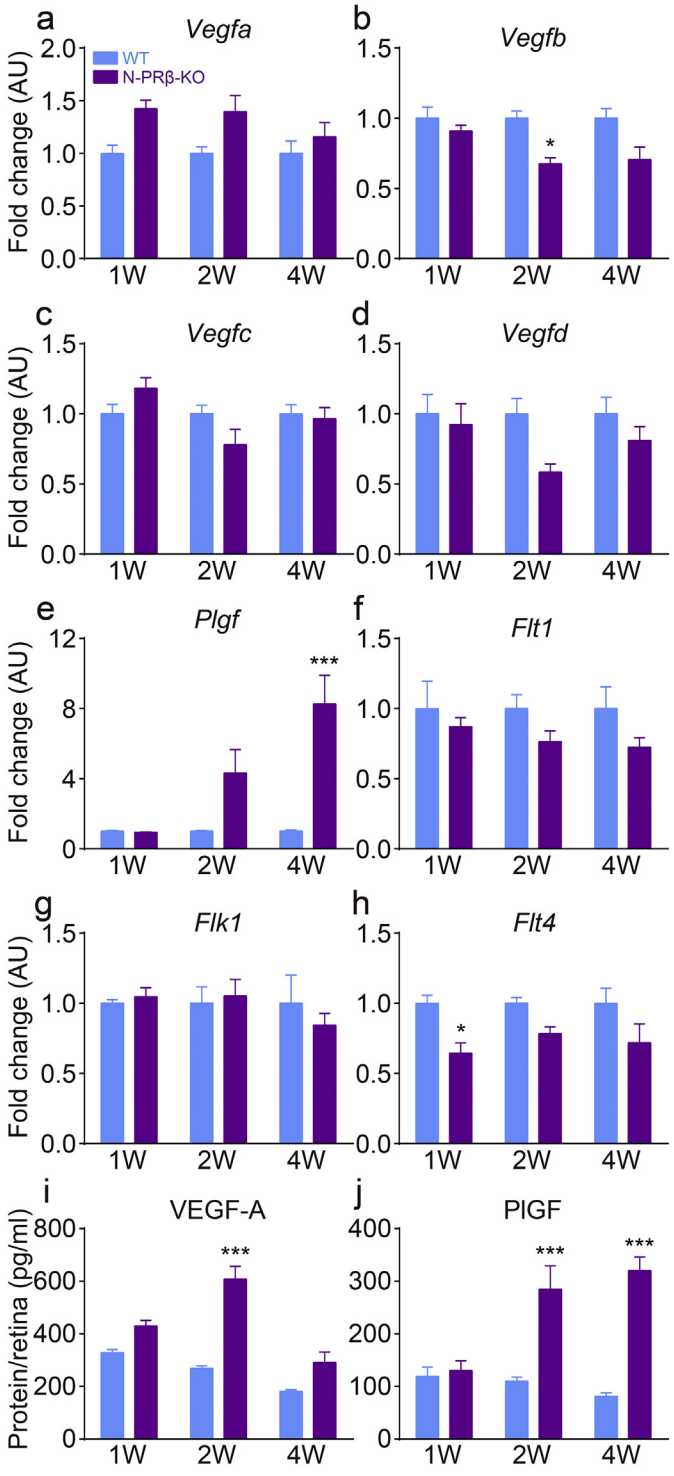

Fig. 6. The molecular mechanisms underlying pathological angiogenesis. (a–e) Real-time PCR analyses of VEGF family ligands. *Vegfa* mRNA (a) expression in N-PRβ-KO mice tended to be higher compared to that of WT mice at 1 and 2 weeks. *Plgf* mRNA (e) expression in N-PRβ-KO mice was gradually upregulated from 2 weeks and was significantly higher at 4 weeks compared to the levels observed in WT mice. *Vegfb* (b), *Vegfc* (c), and *Vegfd* (d) mRNA levels in N-PRβ-KO mice were significantly lower or tended to be lower compared with those of WT mice at all time points. (f–h) Real-time PCR analyses of VEGF family receptors. *Flt1* (f), *Flk1* (g), and *Flt4* (h) mRNA levels in N-PRβ-KO mice were significantly lower or tended to be lower than or comparable to levels observed in WT mice at all time points. n = 8 at the indicated time points. (i and j) ELISA results at 1- to 4-week retinas. VEGF-A expression (i) was significantly higher at 2 weeks in KO mice than WT mice, and decreased at 4 weeks. In N-PRβ-KO mice, PlGF (j) showed significantly higher expression at 2 and 4 weeks compared to the levels observed in WT mice. n = 11–15 at the indicated time points. All values represent means ± SEM. *, $p < 0.05$; ***, $p < 0.001$ vs. WT at the same time points.

damage including proliferative DR pathology in hypomorphic mutations in PDGFRβ or PDGF-B, while the details of proliferative DR pathology were not described [7]. Pericytes that cover cranial vessels derived from either neural crest cells or mesodermal cells emerged around the tube formed endothelial cells, proliferated and migrated along such tubes [1,54]. Accordingly, we chose *Nestin* promoter, a promoter activated in neural crest cells, to target *Pdgfrb* in neural crest-derived pericytes in N-PRβ-KO mice. While considerable number of Nestin-Cre-insensitive PDGFRβ$^+$NG2$^+$αSMA$^+$ pericytes was remaining, Nestin-Cre-sensitive PDGFRβ$^+$NG2$^+$αSMA$^-$ subset of pericytes was mostly depleted, resulting in severe loss of pericyte coverage of retinal capillaries. These may indicate that neural crest-derived pericytes take major part of coverage in retinal blood vessels.

αSMA expressing fibroblasts from an uncertain origin contract extracellular matrix, and are thought to be important for the traction retinal injury [4,27]. In our previous study, the tumor cell-derived PDGF-BB built up a high gradient that attracted PDGFRβ$^+$/NG2$^+$ pericytes to move away from tumor microvessels and transformed into αSMA$^+$/FSP$^+$/PDGFRα$^+$ cancer-associated fibroblasts [24], in which such cellular transition were termed pericyte-fibroblast transition (PFT). Similar PFT was also mediated by macrophage-derived PDGF-BB in an adipose tissue after high-fat diet [34]. In N-PRβ-KO mice, while Nestin-Cre-sensitive PDGFRβ$^+$NG2$^+$αSMA$^-$ pericytes were mostly depleted from retinal capillaries, Nestin-Cre-insensitive PDGFRβ$^+$NG2$^+$αSMA$^+$ pericytes still remained on arterioles and venules. These remaining pericytes, however, did not fully enwrap the microvasculature; instead, detached from blood vessels, eventually loosing NG2 and PDGFRβ expression, and were incorporated into the proliferative membrane. Accordingly, our data indicated, for the first time, that PFT could be, at least in part, the origin of αSMA$^+$ retinal myofibroblasts. PDGFRα$^+$ astrogliosis was another important finding in the retinas of N-PRβ-KO mice. Induced overexpression of PDGF-BB in photoreceptors causes astroglial cell-mediated tractional retinal detachment [42]. PDGF-BB was substantially augmented in the retinas of N-PRβ-KO mice, indicating that PDGF-BB may contribute to tractional retinal detachment via PFT and by astrogliosis, and thus could be an important therapeutic target for the prevention of retinal detachment.

In N-PRβ-KO retinas, PlGF and VEGF-A were significantly upregulated at the progression phase of the disease. Similarly, PlGF and VEGF-A are increased in patients with proliferative DR, and the increases of them were correlated well to each other [28,30,46]. VEGF-A binds VEGFR1 and VEGFR2, and PlGF exclusively binds VEGFR1 [36]. In addition to the angiogenic effects via direct VEGFR1 activation, PlGF can synergistically contribute to angiogenesis and plasma extravasation in pathological conditions together with VEGF-A via several different mechanisms; e.g., in experimental angiogenesis models, PlGF/VEGFR1 bindings freed up VEGF-A to activate VEGFR2, and PlGF/VEGFR1 transphosphorylated VEGFR2 ([5,9]; [13]). After these, the present study of genetic inactivation of VEGFR1 demonstrated the critical role of VEGFR1 in pathological angiogenesis of retinopathy, where PlGF and VEGF-A were increased. Along this line, Aflibercept, a decoy receptor that can bind and inhibit VEGF-A and PlGF, is highly effective with respect to therapeutic outcomes for DR [12]. Correctively, PlGF, VEGF-A, and their shared receptor VEGFR1 are indicated to be a therapeutic target of DR that may restore the normal vascular structures.

Currently, anti-VEGF-A therapy using Ranibizumab, Bevacizumab, Aflibercept and Pegaptanib is the most established treatment for pathological blood vessel formation in DR [8,14,22,38,40]. In addition to this, retinal damage, such as tractional detachment, proliferative membrane formation, and structural destruction, are serious threats for vision loss. In this study, we established a useful mouse retinopathy model that can consistently reproduce proliferative DR. Based on analyses of this retinopathy, PDGF-BB-PDGFRα and PDGFRβ axes are potential therapeutic targets for the prevention of tractional retinal detachment, and suppression of PlGF/VEGF-A-VEGFR1 axis may be a novel therapeutic target and

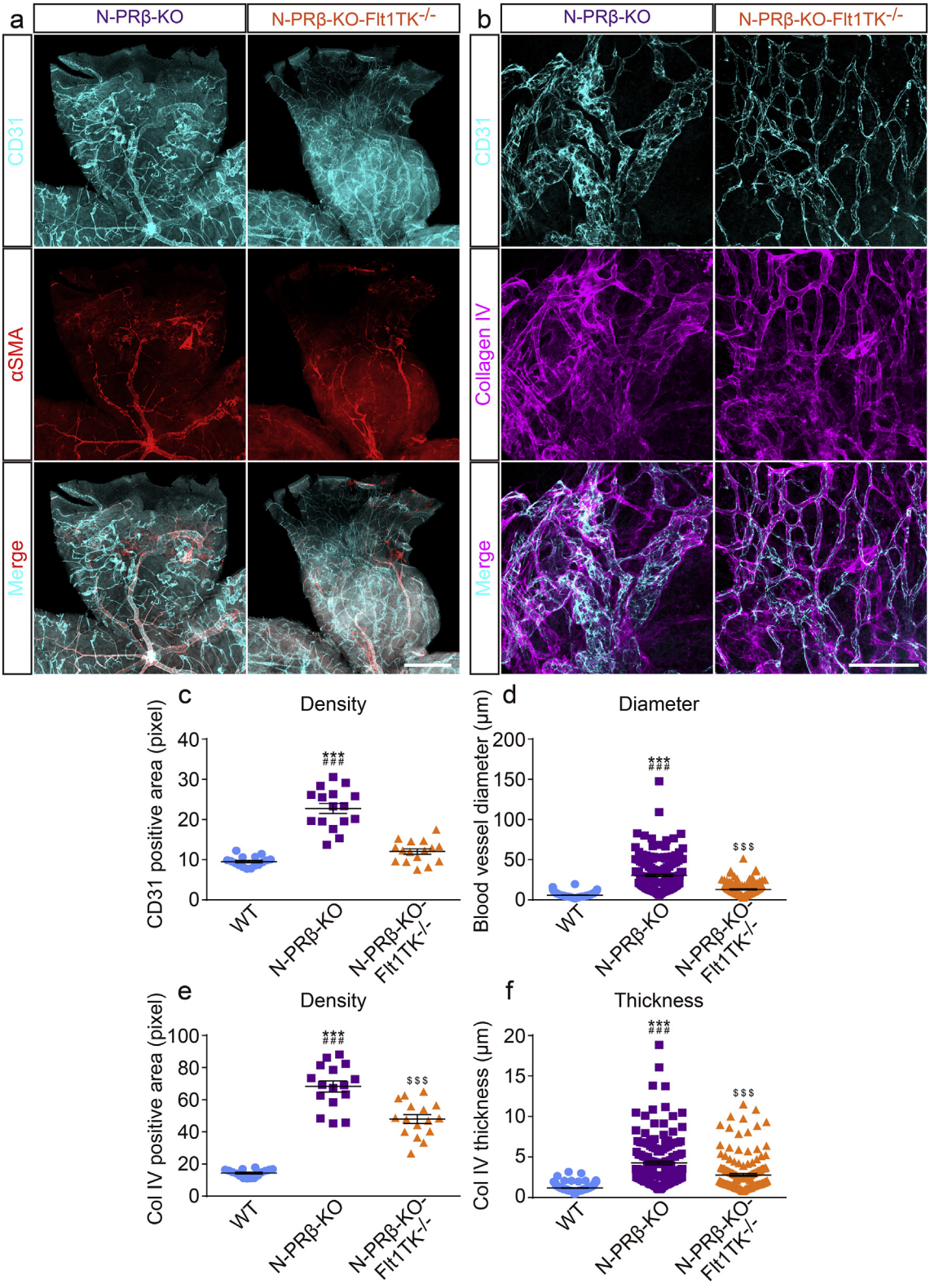

prevent pathological angiogenesis in proliferative DR. Further studies of the sequences of cellular events and interactions among growth factors and cytokines in N-PRβ-KO mice will hopefully facilitate the development of effective DR treatments.

Funding Sources

This work was supported by Grants-in-Aid for Scientific Research JP26460360 (to S.Y.), JP25293093 (to M.S.) and JP15K08396 (to Y.I.),

and the Scientific Research on Innovative Areas JP23122506 (to S.Y.) from The Ministry of Education, Culture, Sports, Science and Technology.

Conflicts of Interest

The authors declare no competing conflicts of interest.

Author Contributions

S.Y. and M. Sasahara conceived and designed the project. H.K., S.K., Y. I., S.Y., T.H., E.A., H.S., T.M., and M. Sasahara performed experiments. S.Y. and M. Sasahara wrote the manuscript with significant input from M. Shibuya and Y.S. All authors reviewed the manuscript. S.Y. is the guarantor of this work and, as such, had full access to all the data in the study and takes responsibility for the integrity of the data and the accuracy of the data analysis.

Acknowledgments

We thank members of the Department of Pathology and Life Science Research Center, University of Toyama for thoughtful discussion and careful animal care.

Appendix A. Supplementary Data

Supplementary data to this article can be found online at https://doi.org/10.1016/j.ebiom.2018.04.021.

References

Ando, K., Fukuhara, S., Izumi, N., Nakajima, H., Fukui, H., Kelsh, R.N., et al., 2016. Clarification of mural cell coverage of vascular endothelial cells by live imaging of zebrafish. Development 143:1328–1339. https://doi.org/10.1242/dev.132654.

Andrae, J., Gallini, R., Betsholtz, C., 2008. Role of platelet-derived growth factors in physiology and medicine. Genes Dev 22:1276–1312. https://doi.org/10.1101/gad.1653708.

Antonetti, D., 2009. Eye vessels saved by rescuing their pericyte partners. Nat Med 15: 1248–1249. https://doi.org/10.1038/nm1109-1248.

Arora, P.D., McCulloch, C.A., 1994. Dependence of collagen remodelling on alpha-smooth muscle actin expression by fibroblasts. J Cell Physiol 159:161–175. https://doi.org/10.1002/jcp.1041590120.

Autiero, M., Waltenberger, J., Communi, D., Kranz, A., Moons, L., Lambrechts, D., et al., 2003. Role of PlGF in the intra- and intermolecular cross talk between the VEGF receptors Flt1 and Flk1. Nat Med 9:936–943. https://doi.org/10.1038/nm884.

Behl, T., Kaur, I., Kotwani, A., 2016. Implication of oxidative stress in progression of diabetic retinopathy. Surv Ophthalmol 61:187–196. https://doi.org/10.1016/j.survophthal.2015.06.001.

Betsholtz, C., 2004. Insight into the physiological functions of PDGF through genetic studies in mice. Cytokine Growth Factor Rev 15:215–228. https://doi.org/10.1016/j.cytogfr.2004.03.005.

Carmeliet, P., 2005. Angiogenesis in life, disease and medicine. Nature 438:932–936. https://doi.org/10.1038/nature04478.

Carmeliet, P., Moons, L., Luttun, A., Vincenti, V., Compernolle, V., De Mol, M., et al., 2001. Synergism between vascular endothelial growth factor and placental growth factor contributes to angiogenesis and plasma extravasation in pathological conditions. Nat Med 7:575–583. https://doi.org/10.1038/87904.

Crawford, T.N., Alfaro 3rd, D.V., Kerrison, J.B., Jablon, E.P., 2009. Diabetic retinopathy and angiogenesis. Curr Diabetes Rev 5, 8–13.

De Falco, S., Gigante, B., Persico, M.G., 2002. Structure and function of placental growth factor. Trends Cardiovasc Med 12, 241–246.

Diabetic Retinopathy Clinical Research, Wells, J.A., Glassman, A.R., Ayala, A.R., Jampol, L.M., Aiello, L.P., et al., 2015. Aflibercept, bevacizumab, or ranibizumab for diabetic macular edema. N Engl J Med 372:1193–1203. https://doi.org/10.1056/NEJMoa1414264.

De Falco, S., 2012. The discovery of placenta growth factor and its biological activity. Exp Mol Med 44:1–9. https://doi.org/10.3858/emm.2012.44.1.025.

Ferrara, N., Kerbel, R.S., 2005. Angiogenesis as a therapeutic target. Nature 438:967–974. https://doi.org/10.1038/nature04483.

Ferrara, N., Houck, K., Jakeman, L., Leung, D.W., 1992. Molecular and biological properties of the vascular endothelial growth factor family of proteins. Endocr Rev 13:18–32. https://doi.org/10.1210/edrv-13-1-18.

Fong, G.H., Rossant, J., Gertsenstein, M., Breitman, M.L., 1995. Role of the Flt-1 receptor tyrosine kinase in regulating the assembly of vascular endothelium. Nature 376:66–70. https://doi.org/10.1038/376066a0.

Gao, Z., Sasaoka, T., Fujimori, T., Oya, T., Ishii, Y., Sabit, H., et al., 2005. Deletion of the PDGFR-beta gene affects key fibroblast functions important for wound healing. J Biol Chem 280:9375–9389. https://doi.org/10.1074/jbc.M413081200.

Gariano, R.F., Gardner, T.W., 2005. Retinal angiogenesis in development and disease. Nature 438:960–966. https://doi.org/10.1038/nature04482.

Geraldes, P., Hiraoka-Yamamoto, J., Matsumoto, M., Clermont, A., Leitges, M., Marette, A., et al., 2009. Activation of PKC-delta and SHP-1 by hyperglycemia causes vascular cell apoptosis and diabetic retinopathy. Nat Med 15:1298–1306. https://doi.org/10.1038/nm.2052.

Hellstrom, M., Kalen, M., Lindahl, P., Abramsson, A., Betsholtz, C., 1999. Role of PDGF-B and PDGFR-beta in recruitment of vascular smooth muscle cells and pericytes during embryonic blood vessel formation in the mouse. Development 126, 3047–3055.

Hiratsuka, S., Minowa, O., Kuno, J., Noda, T., Shibuya, M., 1998. Flt-1 lacking the tyrosine kinase domain is sufficient for normal development and angiogenesis in mice. Proc Natl Acad Sci U S A 95, 9349–9354.

Holash, J., Davis, S., Papadopoulos, N., Croll, S.D., Ho, L., Russell, M., et al., 2002. VEGF-Trap: a VEGF blocker with potent antitumor effects. Proc Natl Acad Sci U S A 99: 11393–11398. https://doi.org/10.1073/pnas.172398299.

Horikawa, S., Ishii, Y., Hamashima, T., Yamamoto, S., Mori, H., Fujimori, T., et al., 2015. PDGFRalpha plays a crucial role in connective tissue remodeling. Sci Rep 5 (17948). https://doi.org/10.1038/srep17948.

Hosaka, K., Yang, Y., Seki, T., Fischer, C., Dubey, O., Fredlund, E., et al., 2016. Pericyte-fibroblast transition promotes tumor growth and metastasis. Proc Natl Acad Sci U S A 113: E5618–5627. https://doi.org/10.1073/pnas.1608384113.

Jadeja, S., Mort, R.L., Keighren, M., Hart, A.W., Joynson, R., Wells, S., et al., 2013. A CNS-specific hypomorphic Pdgfr-beta mutant model of diabetic retinopathy. Invest Ophthalmol Vis Sci 54:3569–3578. https://doi.org/10.1167/iovs.12-11125.

Jo, D.H., Cho, C.S., Kim, J.H., Jun, H.O., Kim, J.H., 2013. Animal models of diabetic retinopathy: doors to investigate pathogenesis and potential therapeutics. J Biomed Sci 20:38. https://doi.org/10.1186/1423-0127-20-38.

Kampik, A., Kenyon, K.R., Michels, R.G., Green, W.R., de la Cruz, Z.C., 1981. Epiretinal and vitreous membranes. Comparative study of 56 cases. Arch Ophthalmol 99, 1445–1454.

Khaliq, A., Foreman, D., Ahmed, A., Weich, H., Gregor, Z., McLeod, D., et al., 1998. Increased expression of placenta growth factor in proliferative diabetic retinopathy. Lab Invest 78, 109–116.

Lai, A.K., Lo, A.C., 2013. Animal models of diabetic retinopathy: summary and comparison. J Diabetes Res 2013:106594. https://doi.org/10.1155/2013/106594.

Mitamura, Y., Tashimo, A., Nakamura, Y., Tagawa, H., Ohtsuka, K., Mizue, Y., et al., 2002. Vitreous levels of placenta growth factor and vascular endothelial growth factor in patients with proliferative diabetic retinopathy. Diabetes Care 25, 2352.

Muramatsu, M., Yamamoto, S., Osawa, T., Shibuya, M., 2010. Vascular endothelial growth factor receptor-1 signaling promotes mobilization of macrophage lineage cells from bone marrow and stimulates solid tumor growth. Cancer Res 70:8211–8221. https://doi.org/10.1158/0008-5472.CAN-10-0202.

Nguyen, Q.D., De Falco, S., Behar-Cohen, F., Lam, W.C., Li, X., Reichhart, N., et al., 2016. Placental growth factor and its potential role in diabetic retinopathy and other ocular neovascular diseases. Acta Ophthalmol https://doi.org/10.1111/aos.13325.

Ogura, S., Kurata, K., Hattori, Y., Takase, H., Ishiguro-Oonuma, T., Hwang, Y., et al., 2017. Sustained inflammation after pericyte depletion induces irreversible blood-retina barrier breakdown. JCI Insight e90905:2. https://doi.org/10.1172/jci.insight.90905.

Onogi, Y., Wada, T., Kamiya, C., Inata, K., Matsuzawa, T., Inaba, Y., et al., 2017. PDGFRbeta regulates adipose tissue expansion and glucose metabolism via vascular remodeling in diet-induced obesity. Diabetes https://doi.org/10.2337/db16-0881.

Fig. 7. Genetical blockade of VEGFR1 signaling alleviates pathological angiogenesis.(a) While abnormal αSMA$^+$ cell migration and proliferation membrane-like structures with retinal detachment can be observed in both genotypes, pathological angiogenesis appears to be normalized N-PRβ-KO-Flt1TK$^{-/-}$ mice compared with N-PRβ-KO mice at 4 weeks. CD31$^+$ blood vessels (cyan) and αSMA$^+$ cells (red). (b) Whereas highly remodeled retinal vasculature is observed in N-PRβ-KO mice, relatively normal blood vessel sizes, vascular networks, and ECM deposition are observed in N-PRβ-KO-Flt1TK$^{-/-}$ mice at 4 weeks. CD31$^+$ blood vessels (cyan) and collagen type IV deposition (magenta). (c and d) The N-PRβ-KO-Flt1TK$^{-/-}$ blood vessel area was significantly smaller than that of N-PRβ-KO mice and similar to that of WT mice (c). $n = 16$ randomly selected areas (20× objective lens) from 4 retinas collected from males and females. The blood vessel diameter of N-PRβ-KO-Flt1TK$^{-/-}$ retinas was significantly smaller than that of N-PRβ-KO retinas and was similar level to WT, but statistically significant (d). $n = 160$ randomly selected blood vessels (20× objective lens) from 4 retinas collected from males and females. (e and f) The collagen type IV deposition in N-PRβ-KO-Flt1TK$^{-/-}$ was significantly smaller than that of N-PRβ-KO mice and significantly larger than that of WT mice (e). n = 16 randomly selected areas (20× objective lens) from 4 retinas collected from males and females. The collagen type IV thickness from endothelial cell surface in N-PRβ-KO-Flt1TK$^{-/-}$ retinas was significantly smaller than that of N-PRβ-KO retinas and significantly larger than that of WT (f). n = 160 randomly selected blood vessels (20× objective lens) from 4 retinas collected from males and females. All values represent means ± SEM. ***, $p < 0.001$ vs. WT at the same time points, $^{\#\#\#}$, $p < 0.001$ vs. N-PRβ-KO-Flt1TK$^{-/-}$, $^{\$\$\$}$, $p < 0.001$ vs. WT. Scale bar = 500 μm (a), 100 μm (b).

Osaadon, P., Fagan, X.J., Lifshitz, T., Levy, J., 2014. A review of anti-VEGF agents for proliferative diabetic retinopathy. Eye (Lond) 28:510–520. https://doi.org/10.1038/eye.2014.13.

Park, J.E., Chen, H.H., Winer, J., Houck, K.A., Ferrara, N., 1994. Placenta growth factor. Potentiation of vascular endothelial growth factor bioactivity, in vitro and in vivo, and high affinity binding to Flt-1 but not to Flk-1/KDR. J Biol Chem 269, 25646–25654.

Park, D.Y., Lee, J., Kim, J., Kim, K., Hong, S., Han, S., et al., 2017. Plastic roles of pericytes in the blood-retinal barrier. Nat Commun 8, 15296. https://doi.org/10.1038/ncomms15296.

Pieramici, D.J., Rabena, M.D., 2008. Anti-VEGF therapy: comparison of current and future agents. Eye (Lond) 22:1330–1336. https://doi.org/10.1038/eye.2008.88.

Praidou, A., Papakonstantinou, E., Androudi, S., Georgiadis, N., Karakiulakis, G., Dimitrakos, S., 2011. Vitreous and serum levels of vascular endothelial growth factor and platelet-derived growth factor and their correlation in patients with non-proliferative diabetic retinopathy and clinically significant macula oedema. Acta Ophthalmol 89:248–254. https://doi.org/10.1111/j.1755-3768.2009.01661.x.

Rudge, J.S., Thurston, G., Davis, S., Papadopoulos, N., Gale, N., Wiegand, S.J., et al., 2005. VEGF Trap as a novel antiangiogenic treatment currently in clinical trials for cancer and eye diseases, and VelociGene- based discovery of the next generation of angiogenesis targets. Cold Spring Harb Symp Quant Biol 70:411–418. https://doi.org/10.1101/sqb.2005.70.052.

Sato, H., Ishii, Y., Yamamoto, S., Azuma, E., Takahashi, Y., Hamashima, T., et al., 2016. PDGFR-β plays a key role in the ectopic migration of neuroblasts in cerebral stroke. Stem Cells 34:685–698. https://doi.org/10.1002/stem.2212.

Seo, M.S., Okamoto, N., Vinores, M.A., Vinores, S.A., Hackett, S.F., Yamada, H., et al., 2000. Photoreceptor-specific expression of platelet-derived growth factor-B results in traction retinal detachment. Am J Pathol 157:995–1005. https://doi.org/10.1016/S0002-9440(10)64612-3.

Shi, H., Zhang, Z., Wang, X., Li, R., Hou, W., Bi, W., et al., 2015. Inhibition of autophagy induces IL-1beta release from ARPE-19 cells via ROS mediated NLRP3 inflammasome activation under high glucose stress. Biochem Biophys Res Commun 463:1071–1076. https://doi.org/10.1016/j.bbrc.2015.06.060.

Shibuya, M., 2013. Vascular endothelial growth factor and its receptor system: physiological functions in angiogenesis and pathological roles in various diseases. J Biochem 153:13–19. https://doi.org/10.1093/jb/mvs136.

Simonavicius, N., Ashenden, M., van Weverwijk, A., Lax, S., Huso, D.L., Buckley, C.D., et al., 2012. Pericytes promote selective vessel regression to regulate vascular patterning. Blood 120:1516–1527. https://doi.org/10.1182/blood-2011-01-332338.

Spirin, K.S., Saghizadeh, M., Lewin, S.L., Zardi, L., Kenney, M.C., Ljubimov, A.V., 1999. Basement membrane and growth factor gene expression in normal and diabetic human retinas. Curr Eye Res 18, 490–499.

Stewart, M.W., 2016. Treatment of diabetic retinopathy: Recent advances and unresolved challenges. World J Diabetes 7:333–341. https://doi.org/10.4239/wjd.v7.i16.333.

Stitt, A.W., Curtis, T.M., Chen, M., Medina, R.J., McKay, G.J., Jenkins, A., et al., 2016. The progress in understanding and treatment of diabetic retinopathy. Prog Retin Eye Res 51:156–186. https://doi.org/10.1016/j.preteyeres.2015.08.001.

Takahashi, H., Shibuya, M., 2005. The vascular endothelial growth factor (VEGF)/VEGF receptor system and its role under physiological and pathological conditions. Clin Sci (Lond) 109:227–241. https://doi.org/10.1042/CS20040370.

Tammela, T., Zarkada, G., Nurmi, H., Jakobsson, L., Heinolainen, K., Tvorogov, D., et al., 2011. VEGFR-3 controls tip to stalk conversion at vessel fusion sites by reinforcing Notch signalling. Nat Cell Biol 13:1202–1213. https://doi.org/10.1038/ncb2331.

Yamamoto, S., Yoshino, I., Shimazaki, T., Murohashi, M., Hevner, R.F., Lax, I., et al., 2005. Essential role of Shp2-binding sites on FRS2α for corticogenesis and for FGF2-dependent proliferation of neural progenitor cells. Proc Natl Acad Sci U S A 102:15983–15988. https://doi.org/10.1073/pnas.0507961102.

Yamamoto, S., Niida, S., Azuma, E., Yanagibashi, T., Muramatsu, M., Huang, T.T., et al., 2015. Inflammation-induced endothelial cell-derived extracellular vesicles modulate the cellular status of pericytes. Sci Rep 5 (8505). https://doi.org/10.1038/srep08505.

Yamamoto, S., Muramatsu, M., Azuma, E., Ikutani, M., Nagai, Y., Sagara, H., et al., 2017. A subset of cerebrovascular pericytes originates from mature macrophages in the very early phase of vascular development in CNS. Sci Rep 7 (3855). https://doi.org/10.1038/s41598-017-03994-1.

Yamanishi, E., Takahashi, M., Saga, Y., Osumi, N., 2012. Penetration and differentiation of cephalic neural crest-derived cells in the developing mouse telencephalon. Dev Growth Differ 54:785–800. https://doi.org/10.1111/dgd.12007.